D2.6 – Report on chemical stability of the coated interconnects

PROJECT INFORMATION

GRANT AGREEMENT NUMBER	826323
PROJECT FULL TITLE	Low Cost Interconnects with highly improved Contact Strength for SOC Applications
PROJECT ACRONYM	LOWCOST-IC
FUNDING SCHEME	FCH-JU2
START DATE OF THE PROJECT	1/1-2019
DURATION	36 months
CALL IDENTIFIER	H2020-JTI-FCH-2018-1
PROJECT WEBSITE	www.lowcost-ic.eu

DELIVERABLE INFORMATION

WP NO.	2
WP LEADER	Chalmers University of Technology
CONTRIBUTING PARTNERS	SMT, APE
NATURE	
AUTHORS	Mareddy Reddy, Jan Froitzheim
CONTRIBUTORS	
CONTRACTUAL DEADLINE	06/30/2020
DELIVERY DATE TO EC	12/08/2020

DISSEMINATION LEVEL

PU	Public	x
PP	Restricted to other programme participants (incl. Commission Services)	
RE	Restricted to a group specified by the consortium (incl. Commission Services)	
CO	Confidential, only for the members of the consortium (incl. Commission Services)	

1 Introduction

Solid oxide fuel cells (SOFC) and Solid oxide electrolyzer cells (SOEC) are drawing tremendous interest due to their potential for power generation and conversion for future energy needs. SOFC is a high temperature electrochemical device that produces electrical energy by converting the chemical energy in H_2 and various hydrocarbons in a clean and efficient way. The same system can be run in regenerative mode to achieve the electrolysis of water and carbon dioxide (CO_2). Thus, excess electricity and heat can be used to produce high purity hydrogen in a highly effective manner. Moreover, the carbon dioxide emissions in the atmosphere can be reduced by electrochemical reduction of CO_2 into value-added chemicals.

Every cell, when operated in a fuel cell mode, produces a voltage of less than 1V. Higher voltages and power output are obtained by stacking the cells together in a series with the help of interconnects. Interconnects are critical components in a SOFC and SOEC, which not only electrically connect individual cells but also separates fuel and air at the cell level. The high operating temperature, combined with rigorous heating and cooling cycles, determines the stringent material requirements for the interconnects. With recent developments in materials and manufacturing, the operating temperatures of a SOFC have been lowered to the range of 600 °C-800 °C, allowing the use of metallic interconnects.

Ferritic stainless steels (FSS) are widely researched for interconnect applications, owing to their thermal expansion coefficient comparable to that of ceramics used in the cell components, high electrical and thermal conductivity, high strength, low cost, and ease of manufacturing. However, using FSS in SOFC presents two major challenges. Firstly, the thermal growth of the chromia scale decreases the electrical conductivity of the interconnect, increasing the electrical resistance across the cell. It may also lead to breakaway corrosion eventually. Secondly, the chromia scale reacts with the H_2O in the air to form volatile Cr^{+6} species, which gets deposited on the cathode, referred to as chromium poisoning[1]. Chromium poisoning inhibits the oxygen reduction reaction on the cathode, resulting in degradation in the electrical performance of the cell.

Steels such as Crofer 22H, Crofer APU, Sanergy HT are produced to address these problems by tailoring the alloy chemistry. This includes increasing the Cr content in the steel to ensure Cr reservoir for long term operation; additions of up to 0,5 % Mn to form a $(Cr,Mn)_3O_4$ spinel, lowering chromium evaporation; and a supplement of rare earth (RE) elements to improve the oxidation resistance and scale adherence. Falk Windisch et al[2], Sachitanand et al[3] showed the oxidation and chromium evaporation properties of these steels in SOFC operating conditions. Despite the improvements in steels, coatings are essential to decrease the chromium evaporation and oxidation kinetics for their application as interconnects[4]. Qu et al[5] and Canovic et al[6] showed the beneficial effect of RE in the coatings, which help in lowering the resistances by suppressing the growth of the chromia scale.

The most commonly reported coatings are either based on perovskite structure[7–9] or based on spinel structure[4, 10–12]. A comprehensive review of the coatings can be found in Ref [12]. Of all the

coatings Co, Mn spinel coatings showed encouraging results in reducing chromium evaporation and decreasing oxidation rate with good electrical conductivity. Moreover, these coatings can be applied in a wide range of techniques such as dip coating[7], atmospheric plasma spray coatings[13] electrophoretic deposition (EPD)[14], aerosol spray deposition, and physical vapor deposition (PVD)[4]. PVD coatings are particularly suitable because they can coat roll to roll in high volume process efficiently. Moreover, the self-healing properties of the metallic PVD coatings allow the steel sheets to be shaped into the interconnect after the coating, lowering logistics and handling costs while streamlining the process[15].

According to Hall et al[16], the interconnects can make up to 45% of the stack manufacturing costs. The steels specifically developed towards the interconnect are more expensive than generic FSS, such as 441, 444, and 430 because of expensive processes and low volume production. Since the coatings are unavoidable, using generic FSS as an interconnect would be a better choice to lower the material costs, making SOFC's attractive for commercial application. To proceed with coated commercial steel combination, the properties and behavior in SOFC conditions must be understood. The objective of this deliverable is to understand the chemical stability and oxidation behavior of uncoated and Ce/Co coated commercial FSS 441, K44M for up to 3000 hours. This is done by studying the oxidation kinetics and chromium evaporation in controlled atmospheres. The oxidation properties are correlated to the microstructure by chemical and morphological analysis in SEM.

2 Materials and Methods

Two ferritic stainless steel sheets, AISI 441 (Sandvik Materials and Technology (SMT)) and K44M (Aperam steel) 0,3 mm thick, were used in this project. The composition of the steels is given in Table 1. The steels were coated with state-of-the-art cerium cobalt coating with 10 nm Ce and 600 nm thick Co layer. The coatings were deposited at SMT using a proprietary Physical Vapor Deposition (PVD) technique suitable for a high-volume roll-to-roll process. The steel sheet coated on both sides was further cut into small coupons of 17 x 15 mm to be placed in the reactor. The coupons are ultrasonically cleaned in acetone and ethanol for 20 minutes each, to remove any contaminants present on the surface. The samples are then weighed before starting the exposure.

Table 1: Composition of uncoated and coated steel substrates.

Wt. %	Fe	Cr	C	Mn	Si	S	P	Ni	Nb	N	Mo	Ti	Co	Cu
441 0,3mm Uncoated	Bal.	17.69	0.017	0.32	0.44	0.001	0.023	0.28	0.036	0.016	0.045	0.015		
441 0,3mm Coated	Bal.	**17.53**	0.016	0.4	0.59	0.0002	0.024	0.15	**0.41**	0.015		0.172		
44M 0.3mm Coated & Uncoated	Bal.	**19.03**	0.015	0.35	0.4	0.0003	0.028	0.179	**0,60**	0.02	**1.86**	0.005	0.026	0.092

All the experiments are conducted at two temperatures, 750 °C and 850 °C. The uncoated samples are exposed for 500 hours, whereas the coated samples are exposed for 3000 hours. The atmosphere around the coupons is designed to simulate the cathode side atmosphere in a real stack. To achieve this, the air around the samples is humidified with 3% H_2O. This is obtained by purging the air through a heated water bath that is further connected to a condenser maintained at a temperature of 24.4 °C. Moreover, the airflow is set at 6000 sml min^{-1} to ensure a flow-independent regime inside the reactor. A porous SiC flow restrictor positioned in front of the samples ensures a uniform flow and minimize the natural convection.

Two types of exposures, isothermal time-resolved chromium evaporation exposure, and discontinuous mass gain exposure, are performed to understand the oxidation kinetics and chromium evaporation behavior of the uncoated and coated steels. The exposures are conducted in two types of tube furnaces, single-zone furnaces, and 3-zone furnaces. The single-zone furnace comprises a hot zone of 2 cm, whereas the 3-zone furnace has a hot zone of 25 cm. Hot zone refers to the area of the maximum temperature inside the furnace (i.e. ±3° from nominal value). The longer hot zone in a 3 zone furnace can accommodate far more coupons at a time compared to three coupons exposed in a single zone furnace. The coupons are placed in an alumina holder along the direction of airflow.

The oxidation kinetics of the uncoated steels are studied in a single zone furnace while the coated specimens are exposed in 3 zone furnaces. The reason for this is the high chromium evaporation of the uncoated steels would influence the corrosion behavior of any samples downstream. This problem is negligible with coated samples. The exposed coupons are removed periodically, cooled to ambient temperature. The mass is recorded before putting the samples back into the furnace. Chromium evaporation exposures are performed only in single zone furnaces where 3 coupons of the same sort are used for each exposure. In-situ chromium evaporation measurements are made using the denuder technique devised by Froitzheim et al[17]. The experimental setup is shown in Fig 1. The gas stream including the vaporized chromium species was passed through a denuder tube coated with Na_2CO_3. Chromium species in the air react with the Na_2CO_3, according to Equation **Error! Reference source not found.**.

$$Na_2CO_3(s) + Cr_2O_2(OH)_2(g) \rightarrow Na_2CrO_4(s) + CO_2(g) \text{ ---- (1)}$$

The denuder tubes are replaced at regular intervals without interfering with the exposure. These denuder tubes are leached with water, and the solution is analyzed using Evolution 60S Thermo Scientific spectrometer to get the time-resolved chromium evaporation of these steels.

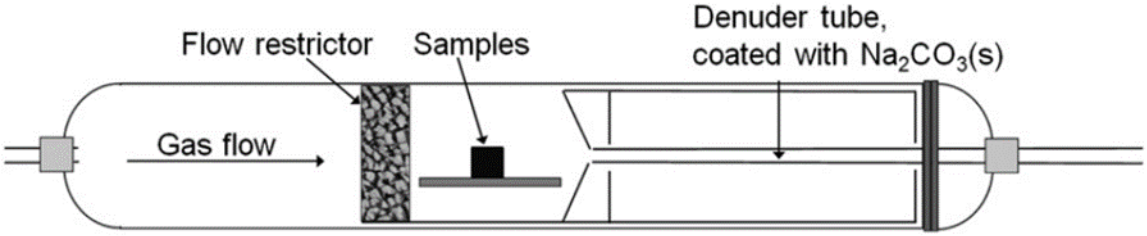

Fig 1: Schematic drawing of the reaction chamber used for the exposures

The microstructure and chemical composition of the exposed coupons is characterized with the help of a JEOL JSM-7800F Prime SEM equipped with an Oxford Instruments Energy Dispersive X-ray spectrometer (EDS).

3 Results and Discussion:

3.1 Discontinuous net mass gains

The net mass gain values of the uncoated steels, K44M, and AISI 441 exposed for 500 hours in the air with 3% H_2O at 750 °C and 850 °C are shown in Fig 2a and Fig 2b, respectively. At 750 °C, AISI 441 showed a small but continuous increase in net mass gain with time. In contrast, K44M showed initial net mass gain during the first 24 hours, followed by a continuous mass loss. Sanergy HT behaved like K44M and Crofer 22H behaved like AISI 441 when exposed to 750 °C in similar conditions[2]. Negative mass gains are associated with para linear oxidation, typically observed at 650 °C in ferritic steels in the presence of humidified air[2, 4]. The net mass gain recorded is the sum of mass gain due to the oxide scale growth and simultaneous mass loss due to oxide scale vaporization[18]. Initially, the oxide scale growth is faster than the simultaneous evaporation, resulting in a positive net mass gain. After a certain limiting oxide scale thickness, the oxide scale does not grow further. However, the oxide scale vaporization continues, resulting in net mass loss. Such a behavior is not observed when the scale growth is much faster compared to the oxide scale vaporization.

Fig 2b shows the net mass gain values of the uncoated coupons at 850 °C. Two major differences are observed in the net mass gains between the two exposure temperatures. Firstly, the mass gains are much lower at 750 °C compared to 850 °C. Secondly, K44M showed an initial mass gain, followed by a continuous mass loss at 750 °C but a continuous mass gain at 850 °C. Both steels, K44M and AISI 441, showed parabolic mass gain with time at 850 °C. However, the steels exhibited differences in the net mass gains, which increased with time. K44M showed a much lower net mass gains compared to AISI 441 at both temperatures. However, one should be cautious in linking these mass gains to oxidation kinetics as chromium evaporation plays a role in determining the net mass gains, explained in section 3.3. Some oxide scale spallation is observed in AISI 441, but not in K44M after 500 hours at 850 °C.

The net mass gain values of the Ce/Co coated steels, K44M, AISI 441, and Crofer APU exposed for 3000 hours in the air with 3% H_2O at 750 °C and 850 °C are shown in Fig 3a and Fig 3b, respectively. Unlike the uncoated steels, all the coated steels showed a continuous net mass gain over time at 750 °C (Fig 3a). Accelerated mass gains are seen in coated samples during the first 24 hours of exposure due to the oxidation of PVD deposited metallic Ce/Co coating. Fig 3b shows the net mass gain values of the coated substrates at 850 °C, which showed increased net mass gain with time. The net mass gains are higher at 850 °C than 750 °C similar to the behavior of the uncoated steels. Large differences in the net mass gains seen in uncoated steels are not found on the coated steels. The difference in the net mass gains between different steels is minimal at the same exposed

temperature. Overall, the coatings were effective in decreasing the oxidation kinetics of the underlying substrate.

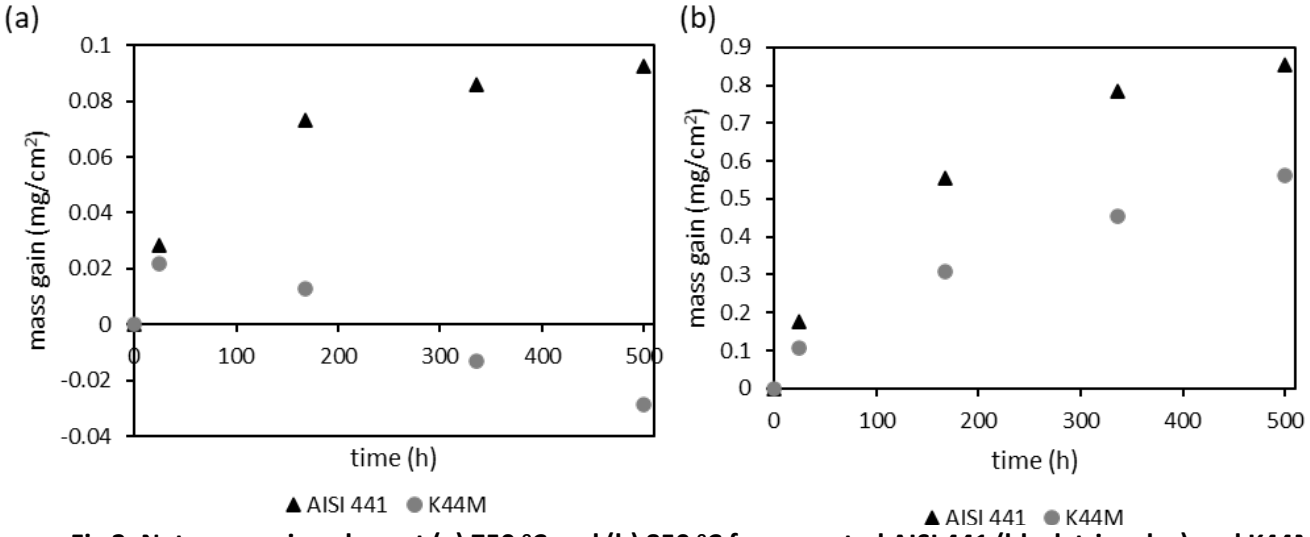

Fig 2: Net mass gain values at (a) 750 °C and (b) 850 °C for uncoated AISI 441 (black triangles) and K44M (grey circles) exposed in air with 3% H_2O for 500 hours.

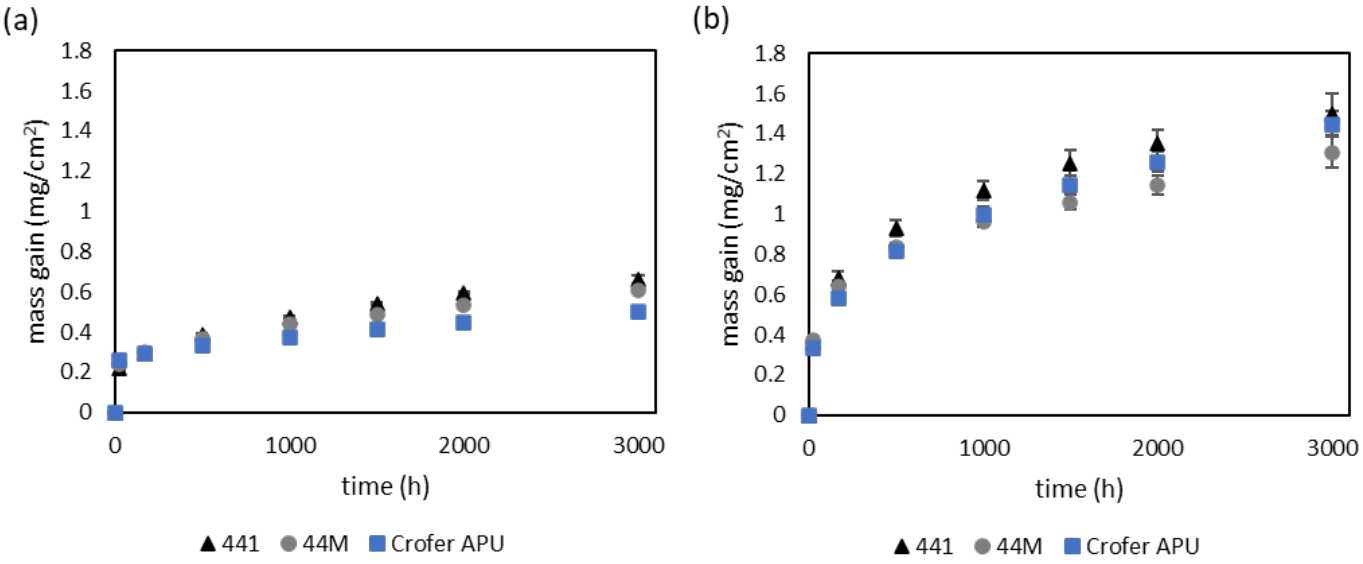

Fig 3: Net mass gain values at (a) 750 °C and (b) 850 °C for Ce/Co coated AISI 441 (black triangles), K44M (grey circles) and Crofer APU (blue squares) exposed in air with 3% H_2O for 3000 hours.

3.2 Chromium evaporation

Fig 4 shows the cumulative chromium evaporation of the uncoated, K44M, and AISI 441 exposed to 750 °C and 850 °C in the air with 3% H_2O. The uncoated steels are exposed for 500 hours, whereas the coated steels are exposed for 1000 hours, continuously. The uncoated steels exhibited dissimilar chromium evaporation behavior at 750 °C (Fig 4a), similar chromium evaporation

behavior at 850 °C (Fig 4b). At 750 °C, uncoated AISI 441 showed a significantly less cumulative chromium evaporation after 500 hours compared to uncoated K44M. The amount of chromium evaporated in 500 hours from uncoated K44M is almost 100% more than on uncoated AISI 441. In contrast, both the steels exhibited similar cumulative chromium evaporation at 850°C. The cumulative chromium evaporation of K44M at 750 °C and 850 °C is similar, while for AISI 441 is lower at 750 °C compared to 850 °C.

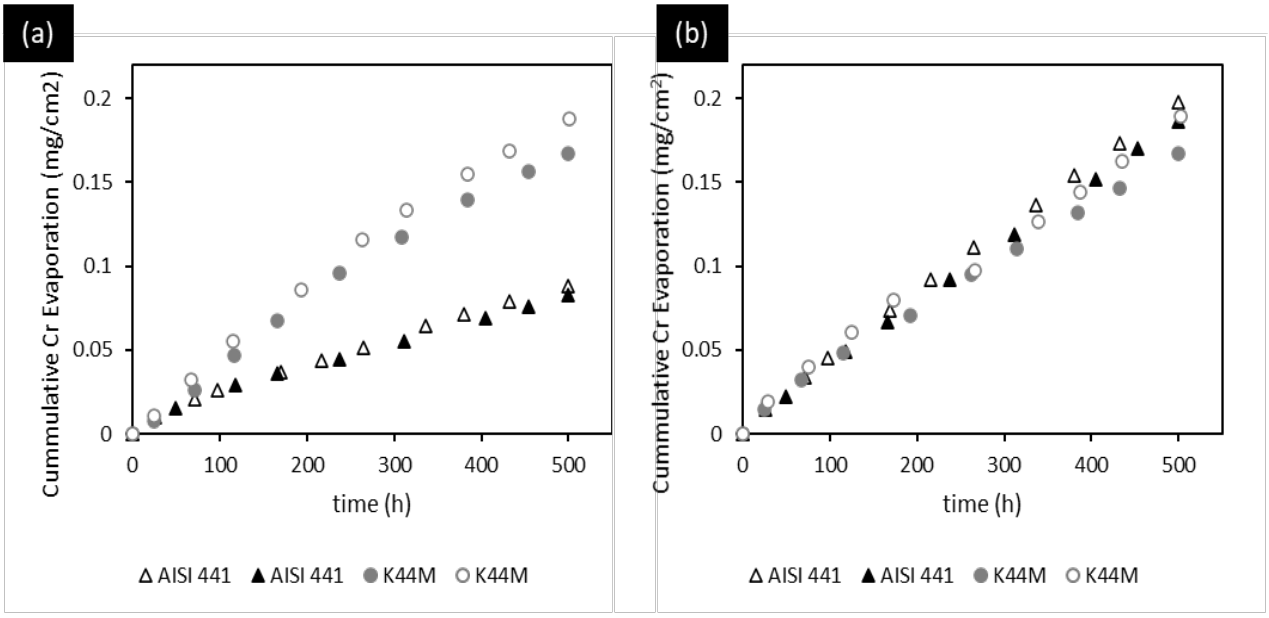

Fig 4: Cumulative chromium evaporation for uncoated steels exposed at (a) 750 °C and (b) 850 °C for uncoated AISI 441 (black triangles) and K44M (grey circles) exposed in air with 3% H_2O for 500 hours. Filled and empty symbols represent two the two individual isothermal exposures

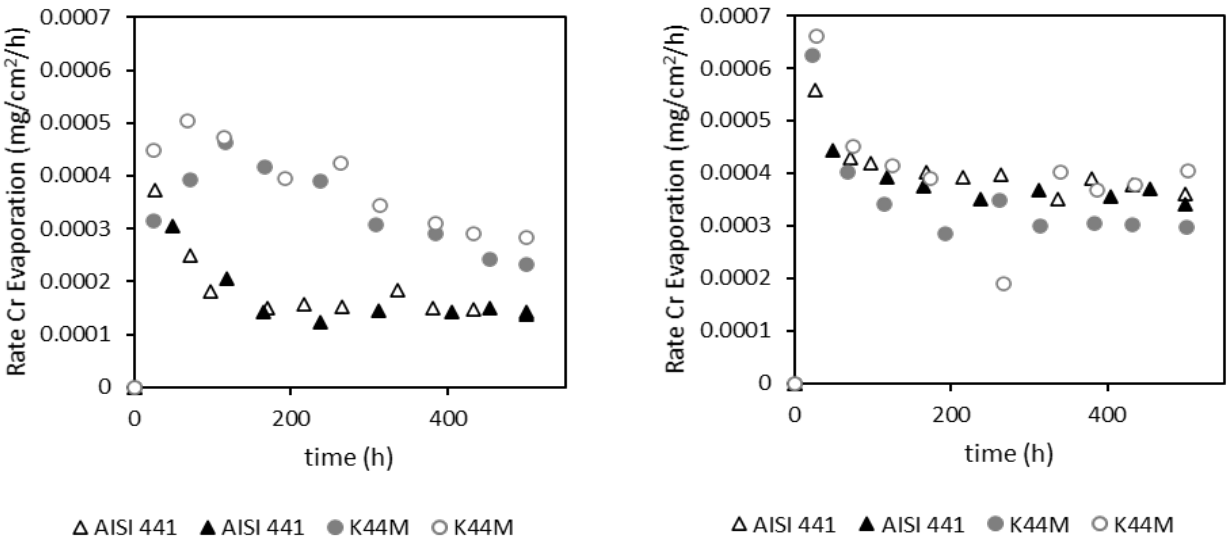

Fig 5: Rate of chromium evaporation as function of time for coated steels exposed at (a) 750 °C and (b) 850 °C for uncoated AISI 441 (black triangles) and uncoated K44M (grey circles) exposed in air with 3% H_2O for 1000 hours. Filled and empty symbols represent two the two individual isothermal exposures

Although the cumulative chromium evaporated is much the same at 750 °C and 850 °C, the rate of chromium evaporation differs significantly with time. Fig 5 shows the rate of chromium evaporation of the uncoated steels at 750 °C and 850 °C. At 750 °C (Fig 5a) in K44M, the rate of chromium evaporation showed a continuous decrease with time; at the same time, the rate is flattened off at 850 °C (Fig 5b) after 150 hours. Nevertheless, the rate of chromium evaporation at the two temperatures is similar after 500 hours. Such behavior of similar chromium evaporation rate at 750 °C and 850 °C is reported on Sanergy HT[2], which also exhibited mass loss when exposed to 750 °C in similar conditions. AISI 441 at 750 °C (Fig 5a) and 850 °C (Fig 5b) showed a decrease in the rate of chromium evaporation during the first 200 hours and later flattened off.

In the coated steels, the cumulative chromium evaporation is considerably lower compared to the uncoated steels. At 750 °C (Fig 6a), the coated K44M showed a 50% higher cumulative chromium evaporation compared to coated AISI 441 after 1000 hours. On the contrary, coated K44M and AISI 441 showed similar cumulative chromium evaporation after 1000 hours at 850 °C (Fig 6b). In summary, coated K44M and coated AISI 441 have similar chromium evaporation at 850 °C and coated K44M exhibits somewhat higher chromium evaporation than coated AISI 441 at 750 °C. The coatings are highly effective in decreasing the chromium evaporation by about 10 times compared to the uncoated samples.

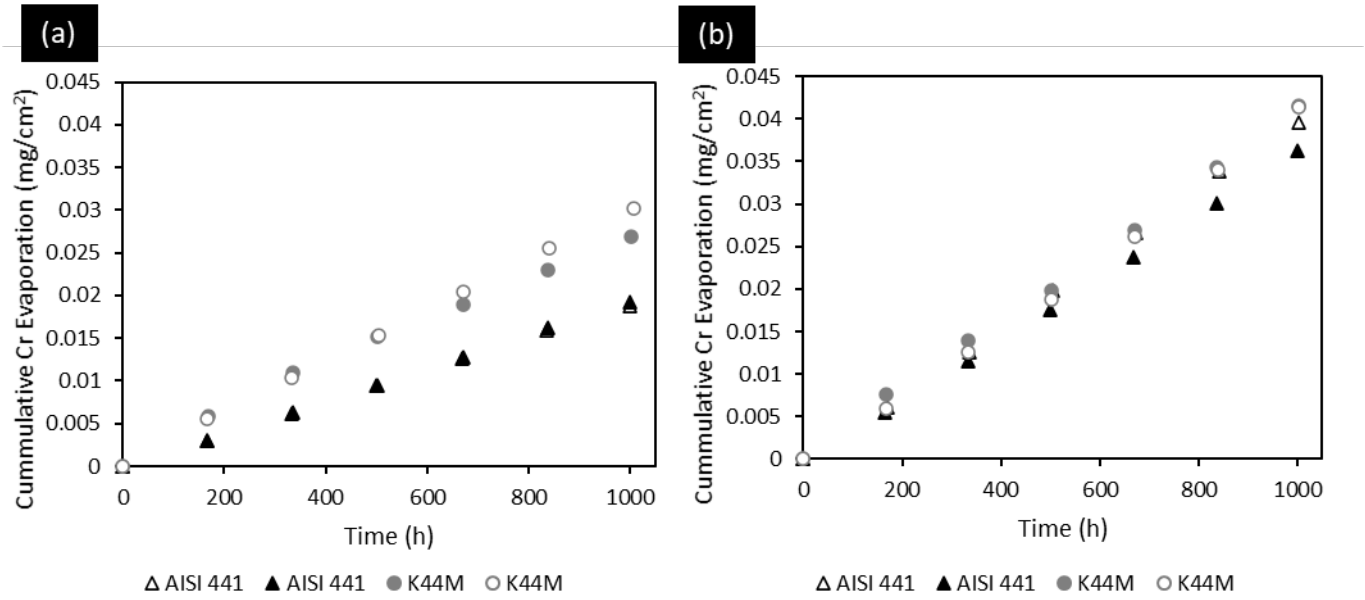

Fig 6: Cumulative chromium evaporation for coated steels exposed at (a) 750 °C and (b) 850 °C for uncoated AISI 441 (black triangles) and K44M (grey circles) exposed in air with 3% H_2O for 1000 hours. Filled and empty symbols represent two the two individual isothermal exposures

Fig 7 shows the chromium evaporation rate of the coated steels as a function of time exposed to 750 °C and 850 °C. The coated steels exposed for 3000 hours in a 3-zone furnace with airflow containing 3% H_2O were subsequently exposed to similar conditions in a single zone furnace to measure the chromium evaporation. At 750 °C (Fig 7a), the rate chromium evaporation is higher in

coated K44M than coated AISI 441 during the first 1000 hours. However, after 3000 hours, both the steels showed a similar rate of chromium evaporation. At 850 °C (Fig 7b), the rate chromium evaporation is similar in both coated steels throughout the time scale. However, the chromium evaporation rate is slightly higher after 3000 hours compared to the evaporation rate until 1000 hours. This is partly due to the spallation of the oxide scale at the uncoated edges after 3000 hours.

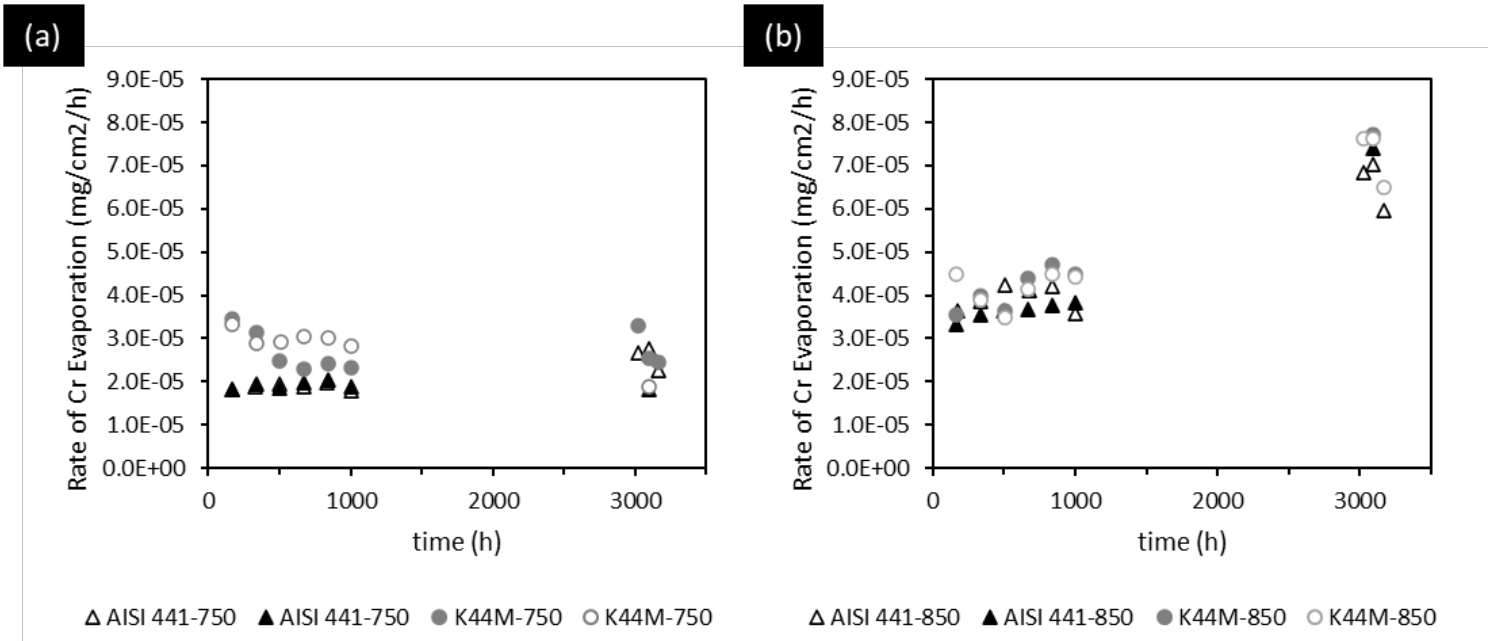

Fig 7: Rate of chromium evaporation as function of time for coated steels exposed at (a) 750 °C and (b) 850 °C for coated AISI 441 (black triangles) and K44M (grey circles) exposed in air with 3% H_2O for 1000 hours. Filled and empty symbols represent two the two individual isothermal exposures. The evaporation values after 3000 hours are for a different set of samples exposed in a 3-zone furnace.

From the data collected, it is apparent that the coatings are highly effective in reducing the chromium evaporation by one order of magnitude. It is worth pointing out that the coated steel coupons used in this work have been cut from a bigger coated steel sheet; thus, the edges of the coupons are uncoated. The uncoated edges of the coated coupons also contribute to the chromium evaporation. As the samples are only 0,3 mm thick, the area of the uncoated edges is only 3.76% of the coated area. Nevertheless, the chromium evaporation on the uncoated coupons is one order of magnitude higher than the coated specimens; the contribution from the uncoated edge cannot be ignored. As a result, the coatings are more effective in reducing chromium evaporation than as stated in this work. Further studies are planned to understand the influence of the uncoated edges on the chromium evaporation.

3.3 Gross mass gains

The net mass gains shown in Fig 2 do not give complete information on the oxidation kinetics of the steels in the exposure conditions. The net mass gains measured are the sum of mass gain due

to oxidation and mass loss due to oxide scale vaporization. To better understand the oxidation kinetics, the net mass gain needs to be corrected, with the amount of Cr_2O_3 evaporated. This gives the total amount of material oxidized, gross mass gain. The amount of Cr_2O_3 evaporated is calculated with the help of the cumulative chromium evaporation values plotted in Fig 4. Further information about this calculation can be found in Sachitanand et al. [3].

Fig 8 shows the gross mass gains of the uncoated steels oxidized at 750 °C and 850 °C. Although uncoated K44M showed mass loss after 500 hours and uncoated AISI 441 showed a small mass gain, both exhibited similar oxidation kinetics at 750 °C (Fig 8a). However, this is not the case at 850 °C (Fig 8b). Uncoated K44M showed much lower corrected mass gain after 500 hours, indicating a better oxidation resistance compared to uncoated AISI 441 at 850 °C. The corrected mass gains of the coated samples are not much different from their net mass gains. The mass loss due to chromium evaporation is one order of magnitude lower than mass gain due to oxidation. This is because of low chromium evaporation on the coated samples.

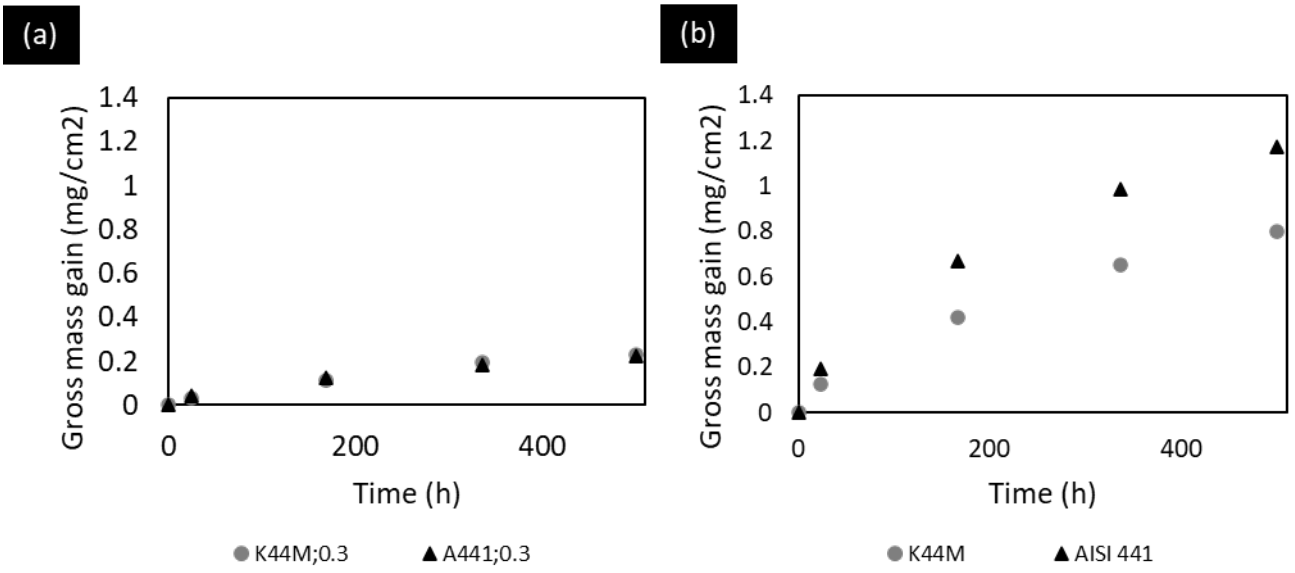

Fig 8: Gross mass gains (corrected for Cr evaporation) of uncoated steels, AISI 441 (black triangles) and K44M (grey circles) exposed in air with 3% H_2O for 500 hours.

3.4 Microstructure

Fig 9 shows the broad ion beam milled cross-section micrographs of the coated steels, K44M, AISI 441 exposed to 750 °C, and 850 °C after 1000 hours. The coatings are intact and showed a continuous oxide scale. At 750 °C, the coated K44M (Fig 9a) showed a slightly wavy oxide scale with coating on the top and chromia scale beneath it. The coating is porous towards the surface. Laves phases are found along the grain boundaries and inside the grain. At 850 °C, the coated K44M (Fig 9b) shows a much wavier oxide scale compared to 750 °C. The coating appeared to be denser, and the thickness of the chromia scale is not homogeneous. The laves phases are found both along the grain boundaries and inside the grains, however, coarser. Laves phases at times are seen at the

metal-oxide interface, at both temperatures. EDX analysis revealed that the laves are comprised of Fe, Nb, Mo, and Si.

The coated AISI 441 at 750 °C (Fig 9c) and 850 °C (Fig 9d) showed a flat oxide scale with coating on the top and chromia scale beneath it. At 750 °C, the coating on AISI 441 appears to be porous as in coated K44M. Ti internal oxidation is seen in AISI 441, which is absent in K44M. Laves phases are seen at both the temperatures, only along the grain boundaries. Laves phases made of Fe, Nb, and Si are coarser at 850°C.The volume fraction of the laves phases is smaller in AISI 441 compared to K44M.

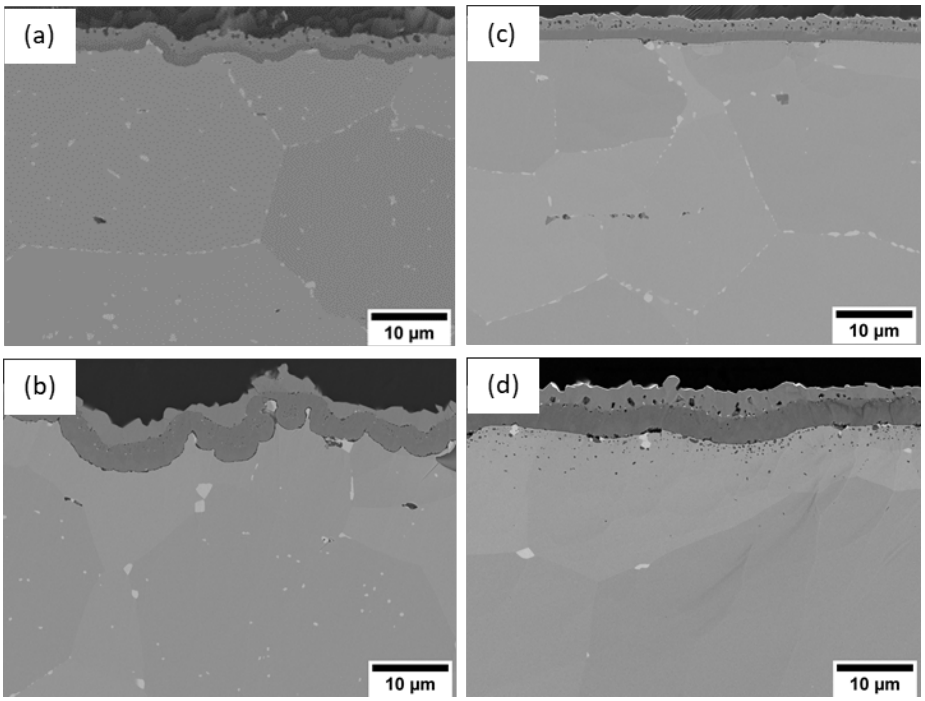

Fig 9: BIB milled crossections of coated steels exposed in air with 3% H_2O for 1000 hours. (a) K44M at 750 °C and (b) K44M at 850 °C; (c) AISI 441 at 750 °C and (d) AISI 441 at 850 °C

Fig 10 shows the micrographs of the coated steels, K44M, AISI 441, Crofer APU exposed at 750 °C, and 850 °C after 3000 hours. All the substrates showed intact coatings with chromia scale beneath the coating. Crofer APU and AISI 441 showed the internal oxidation of Ti next to the metal/oxide interface, but not K44M. K44M and AISI 441 showed the formation of the laves phases in bulk, which are absent in Crofer APU. The laves phases are coarser after 3000 hours compared to 1000 hours. The chromia scale is thinner at 750 °C and thicker at 850 °C, as reflected in their mass gains. The thickness of the chromia scale is uniform, and the oxide scale is flat in AISI 441, while this is not the case with Crofer APU and K44M. K44M showed a wavy oxide scale with a non-uniform thickness of the chromia scale. In the case of Crofer APU, the oxide scale is flatter compared to K44M. However, the thickness of the chromia scale is not uniform. At places, the chromia scale appears to be protruding into the metal. Despite the variation in chromia scale thickness, the average thickness of the chromia scale formed on these steels is similar. The wavy type of the oxide

scale in K44M will be beneficial as it increases the adhesion of the oxide scale. It might be due to internal oxidation of Ti, the oxide scale is flat in Crofer APUand AISI 441.

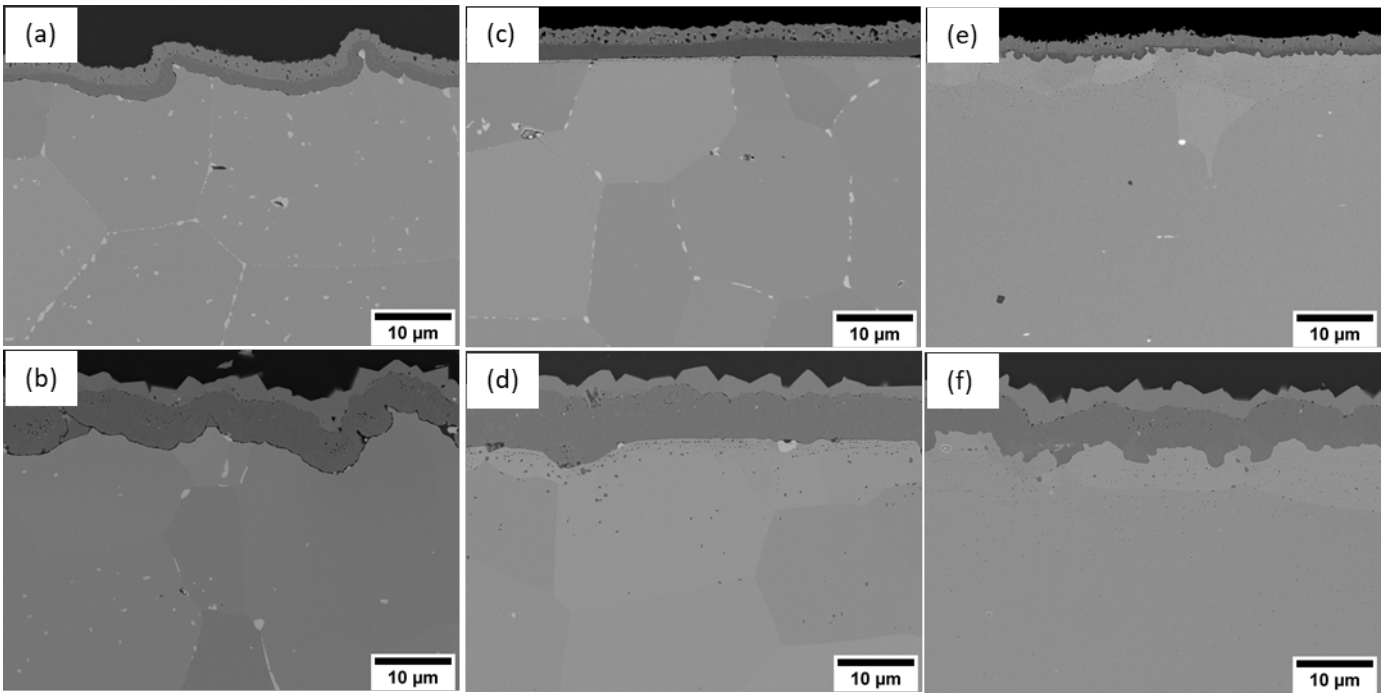

Fig 10: BIB milled crossections of coated steels exposed in air with 3% H_2O for 3000 hours. (a) K44M at 750 °C and (b) K44M at 850 °C; (c) AISI 441 at 750 °C and (d) AISI 441 at 850 °C; (e) Crofer APU at 750 °C and (f) Crofer APU at 850 °C

Fig 11, Fig 12 shows the EDX maps of the coated steels K44M, AISI 441, and Crofer APU exposed in the air with 3% H_2O for 3000 hours at 750 °C and 850 °C respectively. EDX maps for all the samples showed two separate oxide layers. The outermost oxide layer is $(Co,Mn)_3O_4$ spinel. The manganese from the steel diffused into the Co_3O_4 formed on the oxidation of the coating. Further information on the oxidation of coating and formation of $(Co,Mn)_3O_4$ spinel can be found here [6]. Beneath the $(Co,Mn)_3O_4$ spinel is a Cr_2O_3 layer. At the metal-oxide interface, patches of Mn is seen in the chromia layer. It is probably $(Cr,Mn)_3O_4$ spinel, which is also reported in earlier studies on coated FSS[4, 6]. The major differences in the EDX maps between the coated steel sheets in seen on Si maps. In K44M (Fig 11a, Fig 12a), the silica layer appears to be more pronounced at the metal/oxide interface compared to others at both the temperatures. Such a scale is also observed in AISI 441(Fig 11b, Fig 12b); however, with lesser intensity. In Crofer APU (Fig 11c, Fig 12c), it does not exist due to very low silica content in the steel composition. The silica scale at the metal/oxide interface can increase the degradation of the SOFC by increasing the area-specific resistance (ASR) across the steel. This is subject to further investigations.

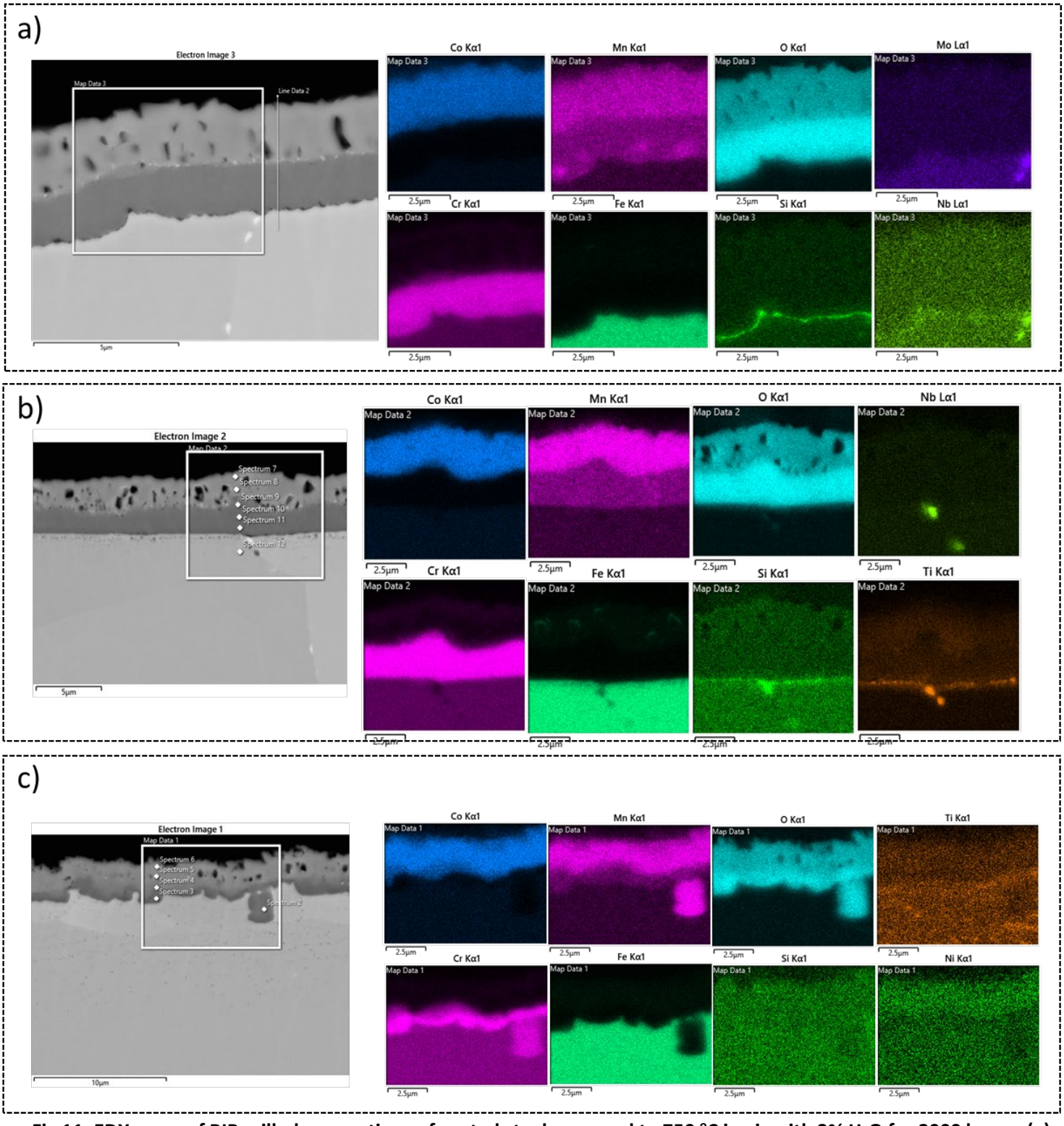

Fig 11: EDX maps of BIB milled crossections of coated steels exposed to 750 °C in air with 3% H_2O for 3000 hours. (a) K44M (b) AISI 441 (c) Crofer APU

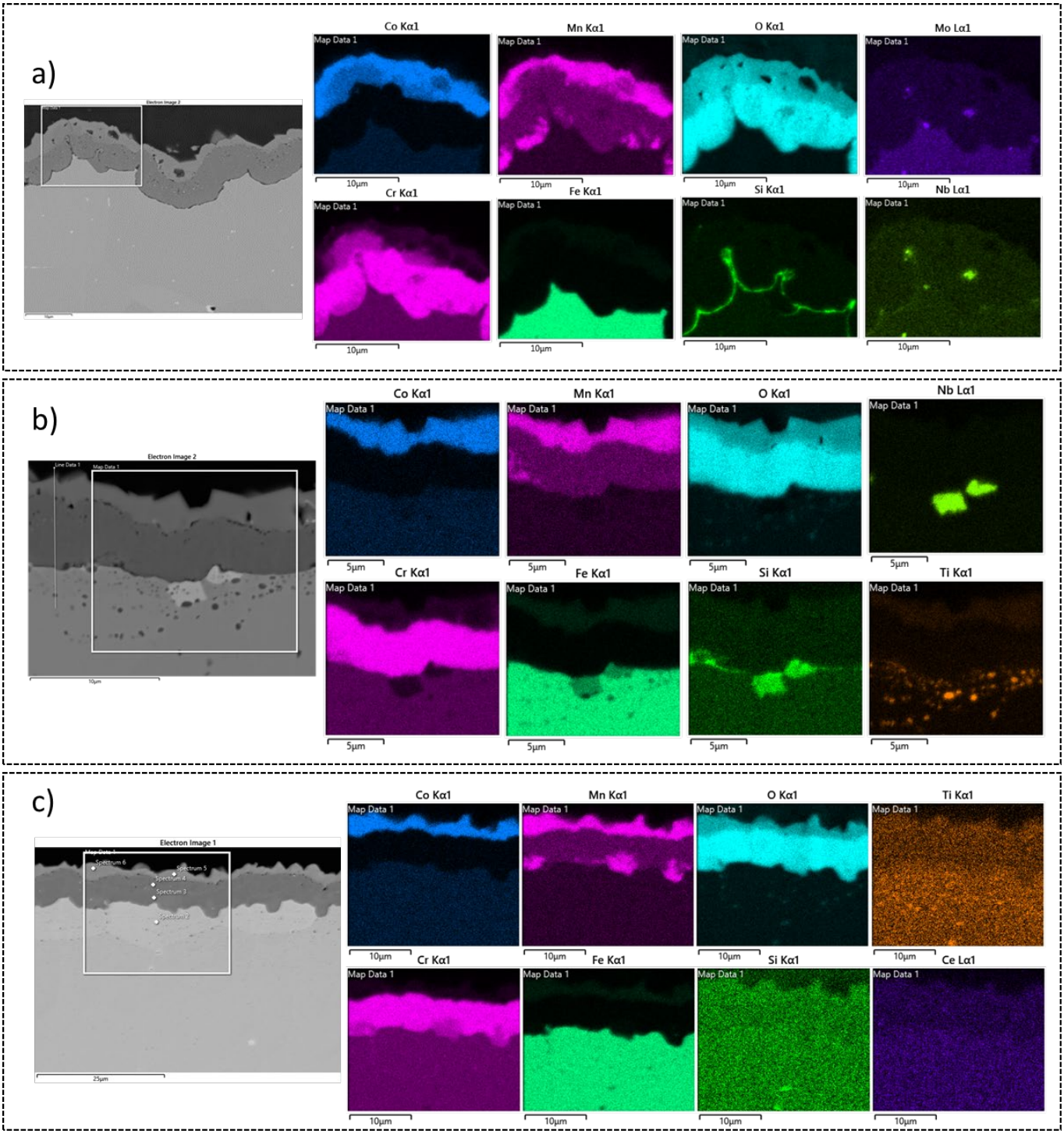

Fig 12: EDX maps of BIB milled crossections of coated steels exposed to 850 °C in air with 3% H_2O for 3000 hours. (a) K44M (b) AISI 441 (c) Crofer APU

4 Conclusion

In this study, the oxidation and chemical stability of the uncoated, Ce/Co coated steels are studied with the help of chromium evaporation, mass gains measurements coupled with microscopy. The uncoated steels showed much higher oxidation kinetics and chromium evaporation compared to the coated steels. K44M showed lower net mass gains than AISI 441 at exposed temperatures. Uncoated K44M showed 100% higher chromium evaporation compared to AISI 441 at 750 °C; however, similar chromium evaporation at 850 °C. Despite the differences in net mass gains and chromium evaporation, the gross mass gains are similar for both uncoated steels at 750 °C. Nevertheless, at 850 °C, the gross mass gains are lower for K44M, indicating superior oxidation resistance in the exposed conditions.

In the coated steels, the mass gains are similar in all the steels irrespective of the exposed temperatures after 3000 hours. The tailored steel, Crofer APU, commercial steels AISI441 and K44M have similar chromia scale thickness after 3000 hours. The coatings are effective in reducing the chromia growth in the steels. The chromium evaporation of coated K44M is slightly higher than coated AISI 441 at 750 °C but similar at 850 °C. Overall, the coatings are very effective in reducing the chromium evaporation on the steels. A pronounced silica scale at the metal/oxide interface is found on K44M but, to a lesser extent, is also observed in AISI 441. The silica scale seems to be thicker at higher temperatures. Such a silica scale is not observed at the metal/oxide in Crofer 22 APU irrespective of the exposed temperature. The silica layer can increase the ASR, increasing the degradation of the stack. .

5 References

1. Jiang SP, Chen X. Chromium deposition and poisoning of cathodes of solid oxide fuel cells - A review. *Int J Hydrogen Energy*. 2014;39(1):505–531. https://doi.org/10.1016/j.ijhydene.2013.10.042
2. Falk-Windisch H, Svensson JE, Froitzheim J. The effect of temperature on chromium vaporization and oxide scale growth on interconnect steels for Solid Oxide Fuel Cells. *J Power Sources*. 2015;287:25–35. https://doi.org/10.1016/j.jpowsour.2015.04.040
3. Sachitanand R, Sattari M, Svensson JE, Froitzheim J. Evaluation of the oxidation and Cr evaporation properties of selected FeCr alloys used as SOFC interconnects. *Int J Hydrogen Energy*. 2013;38(35):15328–15334. https://doi.org/10.1016/j.ijhydene.2013.09.044
4. Falk-Windisch H, Claquesin J, Sattari M, Svensson JE, Froitzheim J. Co- and Ce/Co-coated ferritic stainless steel as interconnect material for Intermediate Temperature Solid Oxide Fuel Cells. *J Power Sources*. 2017;343:1–10. https://doi.org/10.1016/j.jpowsour.2017.01.045
5. Qu W, Jian L, Ivey DG, Hill JM. Yttrium, cobalt and yttrium/cobalt oxide coatings on ferritic stainless steels for SOFC interconnects. *J Power Sources*. 2006;157(1):335–350. https://doi.org/10.1016/j.jpowsour.2005.07.052
6. Canovic S, Froitzheim J, Sachitanand R, *et al.* Oxidation of Co- and Ce-nanocoated FeCr

steels: A microstructural investigation. *Surf Coatings Technol*. 2013;215:62–74. https://doi.org/10.1016/j.surfcoat.2012.08.096
7. Kurokawa H, Jacobson CP, DeJonghe LC, Visco SJ. Chromium vaporization of bare and of coated iron-chromium alloys at 1073 K. *Solid State Ionics*. 2007;178(3–4):287–296. https://doi.org/10.1016/j.ssi.2006.12.010
8. Chevalier S, Valot C, Bonnet G, Colson JC, Larpin JP. The reactive element effect on thermally grown chromia scale residual stress. *Mater Sci Eng A*. 2003;343(1–2):257–264. https://doi.org/10.1016/S0921-5093(02)00359-3
9. Yang Z, Xia GG, Wang CM, *et al.* Investigation of iron-chromium-niobium-titanium ferritic stainless steel for solid oxide fuel cell interconnect applications. *J Power Sources*. 2008;183(2):660–667. https://doi.org/10.1016/j.jpowsour.2008.05.037
10. Talic B, Hendriksen PV, Wiik K, Lein HL. Thermal expansion and electrical conductivity of Fe and Cu doped MnCo2O4 spinel. *Solid State Ionics*. 2018;326:90–99. https://doi.org/10.1016/j.ssi.2018.09.018
11. Goebel C, Berger R, Bernuy-Lopez C, Westlinder J, Svensson JE, Froitzheim J. Long-term (4 year) degradation behavior of coated stainless steel 441 used for solid oxide fuel cell interconnect applications. *J Power Sources*. 2020;449. https://doi.org/10.1016/j.jpowsour.2019.227480
12. Mah JCW, Muchtar A, Somalu MR, Ghazali MJ. Metallic interconnects for solid oxide fuel cell: A review on protective coating and deposition techniques. *Int J Hydrogen Energy*. 2017;42(14):9219–9229. https://doi.org/10.1016/j.ijhydene.2016.03.195
13. Spotorno R, Piccardo P, Perrozzi F, Valente S, Viviani M, Ansar A. Microstructural and Electrical Characterization of Plasma Sprayed Cu-Mn Oxide Spinels as Coating on Metallic Interconnects for Stacking Solid Oxide Fuel Cells. *Fuel Cells*. 2015;15(5):728–734. https://doi.org/10.1002/fuce.201400189
14. Talic B, Wulff AC, Molin S, Andersen KB, Zielke P, Frandsen HL. Investigation of electrophoretic deposition as a method for coating complex shaped steel parts in solid oxide cell stacks. *Surf Coatings Technol*. 2019;380. https://doi.org/10.1016/j.surfcoat.2019.125093
15. Falk-Windisch H, Sattari M, Svensson JE, Froitzheim J. Chromium vaporization from mechanically deformed pre-coated interconnects in Solid Oxide Fuel Cells. *J Power Sources*. 2015;297:217–223. https://doi.org/10.1016/j.jpowsour.2015.07.085
16. Hall TD, McCrabb H, Wu J, Zhang H, Liu X, Taylor J. Electrodeposition Of CoMn Onto Stainless Steels Interconnects For Increased Lifetimes In SOFCs. ECS; 2011:2489–2502. https://doi.org/10.1149/1.3570247
17. Froitzheim J, Ravash H, Larsson E, Johansson LG, Svensson JE. Investigation of Chromium Volatilization from FeCr Interconnects by a Denuder Technique. *J Electrochem Soc*. 2010;157(9):B1295. https://doi.org/10.1149/1.3462987
18. Pujilaksono B, Jonsson T, Halvarsson M, Panas I, Svensson JE, Johansson LG. Paralinear oxidation of chromium in O 2 + H 2O environment at 600-700 °c. *Oxid Met*. 2008;70(3–4):163–188. https://doi.org/10.1007/s11085-008-9114-1

Acknowledgment

This project has received funding from the Fuel Cells and Hydrogen 2 Joint Undertaking under grant agreement No 826323. This Joint Undertaking receives support from the European Union's Horizon 2020 research and innovation programme, Hydrogen Europe and Hydrogen Europe research.